

Fragment Ligands of the m<sup>6</sup>A-RNA Reader YTHDF2

Francesco Nai, Raed Nachawati, František Zálešák, Xiang Wang, Yaozong Li,\* and Amedeo Caffisch\*

Cite This: *ACS Med. Chem. Lett.* 2022, 13, 1500–1509

Read Online

ACCESS |



Metrics &amp; More

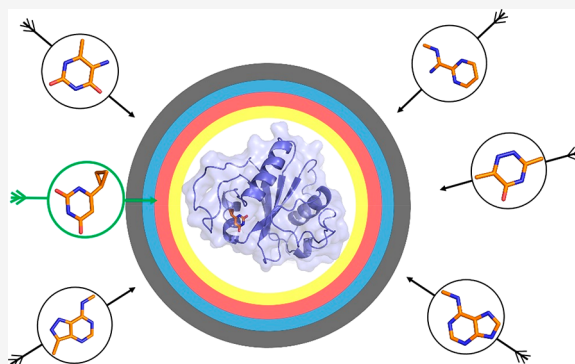


Article Recommendations



Supporting Information

**ABSTRACT:** We report 17 small-molecule ligands that compete with N<sup>6</sup>-methyladenosine (m<sup>6</sup>A) for binding to the m<sup>6</sup>A-reader domain of YTHDF2 (YT521-B homology domain family 2). We determined their binding mode at high resolution by X-ray crystallography and quantified their affinity by a fluorescence-based binding assay. 6-Cyclopropyluracil and a pyrazolopyrimidine derivative have favorable ligand efficiencies of 0.47 and 0.38 kcal mol<sup>-1</sup> per non-hydrogen atom, respectively. They represent useful starting points for hit optimization.



**KEYWORDS:** epitranscriptomics, m<sup>6</sup>A readers, human YTHDF binders, fragment-based drug discovery, in silico molecular design, HTRF binding assays, X-ray crystallography

In 2012, the invention of a new method to map RNA modifications led to the birth of the epitranscriptomics field<sup>1</sup> and, subsequently, to the definition of new protein families, functions, and targets. There are three main classes of epitranscriptome proteins: writer, eraser, and reader proteins.<sup>2</sup> YTH domain-containing family protein 2 (YTHDF2) recognizes RNA with the N<sup>6</sup>-methyladenosine (m<sup>6</sup>A) modification.<sup>3–5</sup> In humans, YTHDF2 is one of the five m<sup>6</sup>A reader proteins: YTH domain containing 1 (YTHDC1), YTHDC2, and YTHDF1–YTHDF3.<sup>6</sup> YTHDF2 shares with the other members of its family a structurally conserved C-terminal YTH domain which is deputed to RNA binding and m<sup>6</sup>A recognition.<sup>7,8</sup>

YTHDF2 takes part in several regulatory processes, from progenitor cell specification<sup>9</sup> to the regulation of inflammatory and cell stress responses,<sup>10</sup> and seems to do so, at least partially, through its involvement in the degradation of m<sup>6</sup>A-containing mRNA.<sup>5</sup> YTHDF2 exerts control on RNA decay by both the YTH-domain and the N-terminal region of the protein. After the YTH domain binds the methylated RNA, multiple sites in the N-terminal region are involved in the recruitment of the CCR4-NOT complex which mediates the degradation of the mRNA polyadenine tail and triggers deadenylation-dependent mRNA decay.<sup>8,11</sup>

YTHDF2 appears to be critically involved in a variety of human cancers, including hepatocellular carcinoma,<sup>12,13</sup> prostate cancer,<sup>14,15</sup> multiple myeloma,<sup>16</sup> and MYC-driven breast cancer,<sup>17</sup> as well as leukemic stem cell development and acute myeloid leukemia initiation and propagation.<sup>18,19</sup> Additionally, YTHDF2 seems to create, with the m<sup>6</sup>A writer methyltransferase-like 3–14 (METTL3–14),<sup>20</sup> a regulatory

axis (renamed METTL3/YTHDF2 m<sup>6</sup>A axis<sup>21</sup>) involved in the tumorigenesis of colorectal carcinoma,<sup>22</sup> bladder cancer,<sup>21</sup> and intrahepatic cholangiocarcinoma.<sup>23</sup>

The development of inhibitors toward epitranscriptomic targets is at its dawn, and only a few papers have been published in this regard.<sup>24–30</sup> Moreover, METTL3 is the only epitranscriptomic target for which high potency and selective inhibitors have been presented.<sup>24,25,28</sup> About 60 small-molecule ligands (micromolar affinity) of the YTHDC1 m<sup>6</sup>A reader domain have been reported,<sup>26,29,30</sup> while no ligand of the three YTHDF domains has been disclosed as of today. Thus, the novelty of the field and the involvement of YTHDF2 in the regulation of mRNA lifetime<sup>5</sup> and tumorigenesis<sup>12–19,21–23</sup> make YTHDF2 an exciting and promising target for the design of chemical probes and anticancer drugs. Additionally, its role as a downstream effector in METTL3/YTHDF2 m<sup>6</sup>A axis-driven cancers<sup>21–23</sup> could make YTHDF2 a superior target to METTL3 for this subset of tumors, limiting the chance of off-targets and side effects.

The targeting of single members of the YTH-family is notoriously difficult due to the similarity of their binding sites.<sup>4,31</sup> Additional structural studies<sup>7,32,33</sup> suggest that binding site conservation is even higher among the YTHDF protein

Received: July 1, 2022

Accepted: August 11, 2022

Published: August 17, 2022



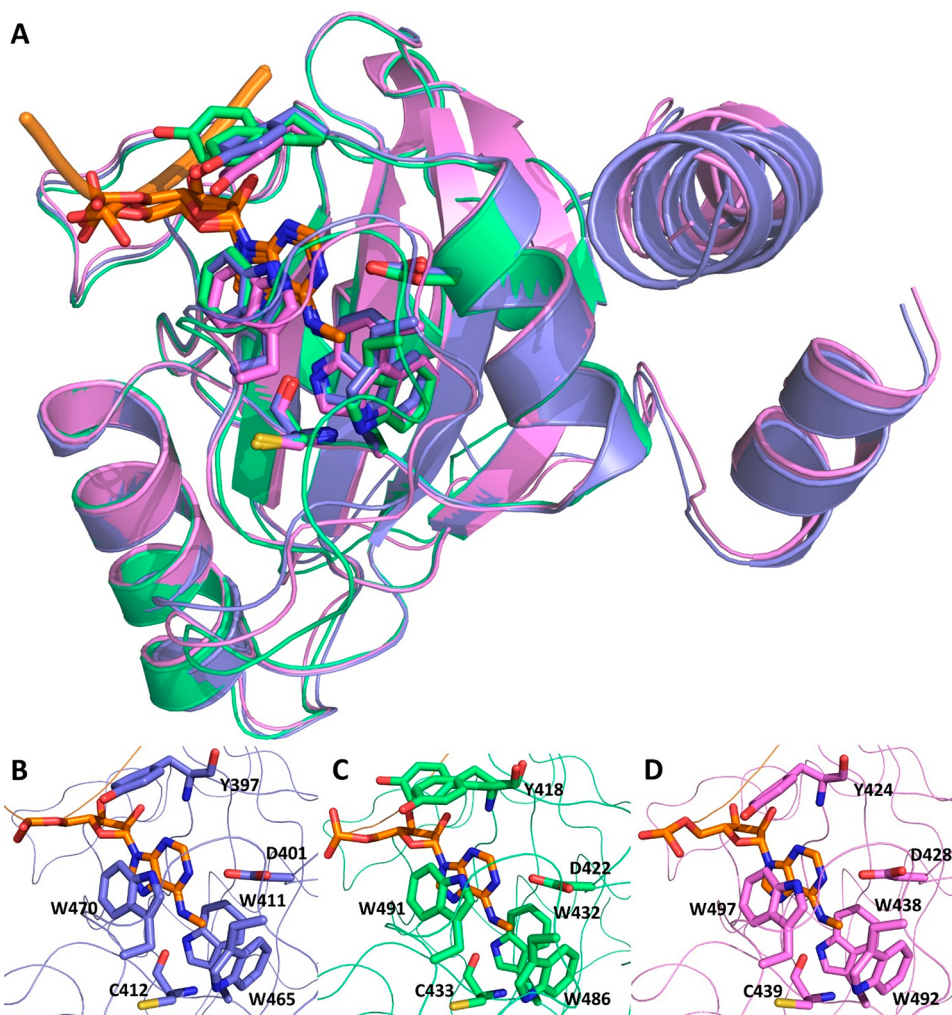


**Figure 1.** Crystal structures of the human YTHDF readers. (A) Structural overlap and (B–D) m<sup>6</sup>A binding site of the reader domain of YTHDF1 (slate, PDB code: 4RCJ), YTHDF2 (lime green, 7Z26), and YTHDF3 (violet, 6ZOT) in complex with m<sup>6</sup>A (orange).

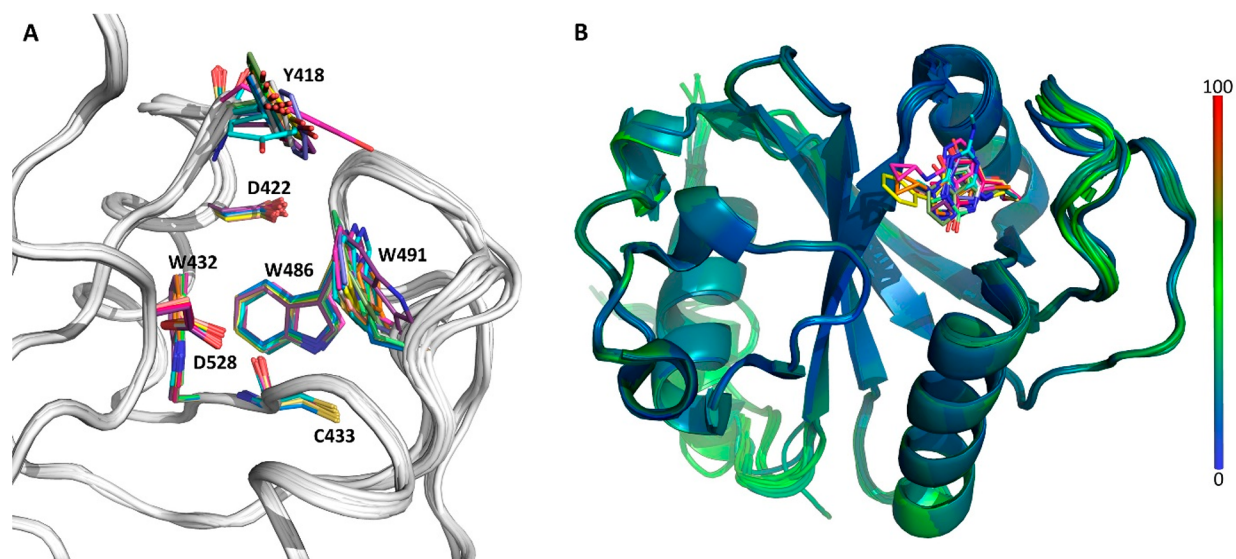


**Figure 2.** Binding site and loop flexibility in the 17 crystal structures of the holo m<sup>6</sup>A reader domain of YTHDF2. (A) Side chains in the m<sup>6</sup>A binding pocket. The 17 fragments are not shown. (B) Structural overlap of the backbone colored according to crystallographic B-factors (from blue to red). The 17 fragments are shown in different colors. The structural overlap was performed using the C $\alpha$  atoms. PDB codes of the 17 structures are listed in Table 1.

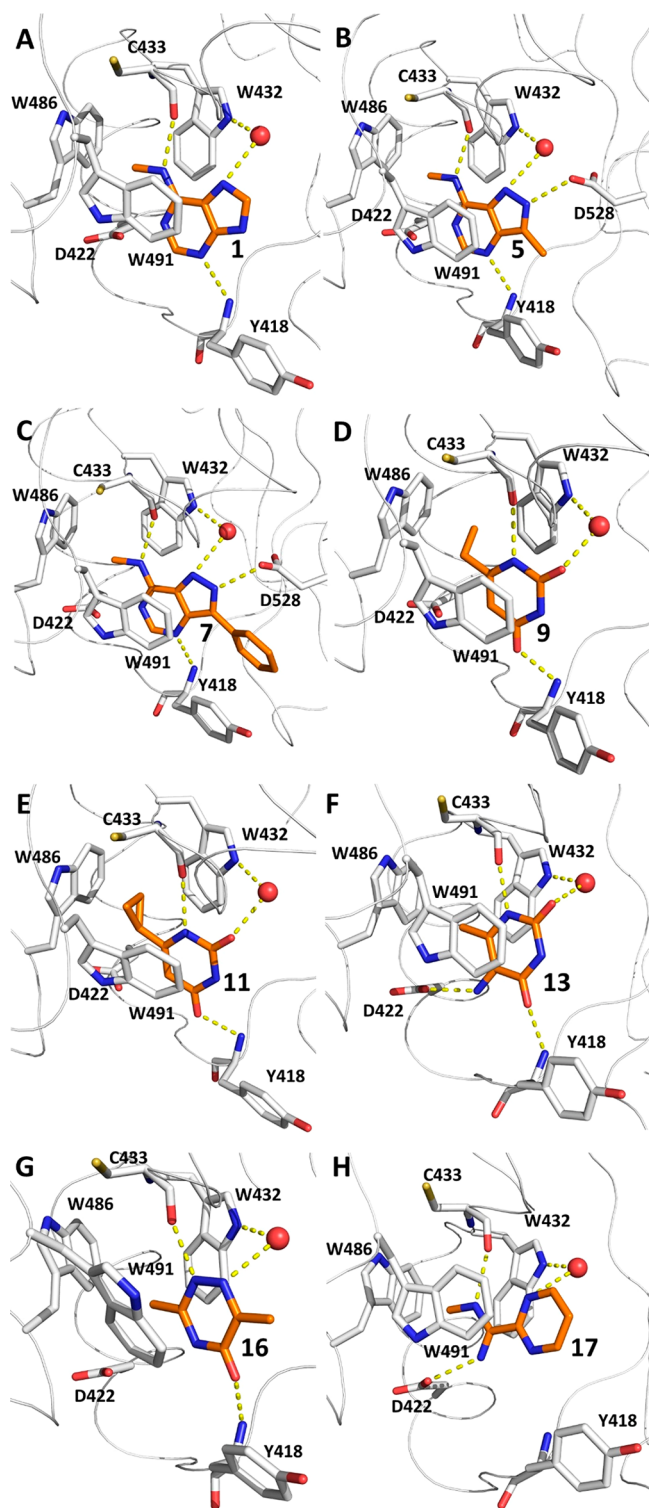


**Figure 3.** Crystal structures of eight ligand-YTHDF2 complexes. (A–H) Binding modes of compounds **1** (PDB code: 7YWB), **5** (7ZSM), **7** (7YXE), **9** (7YX6), **11** (7R5W), **13** (7R5F), **16** (7R5L), and **17** (7ZG4), respectively. The carbon atoms of the ligands are in orange and those of the protein in white. The conserved water molecule (red sphere) and the hydrogen bonds (yellow dashed lines) are emphasized.

family members. The structures of YTHDF1<sup>33</sup> (PDB code: 4RCJ) and YTHDF3<sup>32</sup> (PDB code: 6ZOT) in complex with the recognition motif GG(m<sup>6</sup>A)CU oligoribonucleotide

(oligoRNA) were published in 2015 and 2020, respectively. The structure of YTHDF2 in complex with m<sup>6</sup>A has been available since 2014 (ref 7; PDB code: 4RDN). In contrast, no structure of YTHDF2 bound to oligoRNA has been reported as of today. To allow a complete comparison of the binding sites of the three members of the YTHDF family, we have solved the structure of YTHDF2 in complex with GG(m<sup>6</sup>A)-CU-RNA (PDB code: 7Z26). The overlap of the three structures highlights the high degree of similarity among the YTHDF binding sites, the very similar conformation adopted by their recognition loops<sup>30</sup> as well as the nearly identical position of the RNA backbone [Figure 1A]. Moreover, the position of the solvent-exposed cytosine is characterized by only minimal variations. Higher flexibility can be observed for the guanosines preceding m<sup>6</sup>A in the YTHDF1 and YTHDF3 structures. This observation is consistent with the absence of electron density in the corresponding region of RNA in the complex with YTHDF2.

The binding mode of the methylated adenosine is confirmed to be identical in the three structures [Figure 1B, C, D]. In detail: the YTHDF binding site is constituted by an aromatic tryptophan cage able to tightly accommodate m<sup>6</sup>A. Two tryptophan residues (W491 and W432 in YTHDF2; W497 and W438 in YTHDF3; W470 and W411 in YTHDF1) assume a parallel orientation, with the adenine ring interacting through  $\pi$ -stacking. A third tryptophan (W486 in YTHDF2; W492 in YTHDF3; W465 in YTHDF1) is involved in CH– $\pi$  interactions with the methyl group of m<sup>6</sup>A. Additionally, hydrogen bonds are formed between the backbone carbonyl group of a cysteine (C433 in YTHDF2; C439 in YTHDF3; C412 in YTHDF1) and the N6 of the adenine ring and between the backbone NH group of a tyrosine (Y418 in YTHDF2; Y424 in YTHDF3; Y397 in YTHDF1) and the N3 of the adenine ring. Interestingly, the Y418 side chain of YTHDF2 can assume two different orientations [Figure 1C], and in one of them it seems to engage the O4 of the adenosine ribose in a lone pair– $\pi$  interaction.

Altogether, these observations confirm the very strong conservation of the human YTHDF binding site and its RNA binding mode, also implying the impossibility of designing selective binders for just one of the three human YTHDF proteins based solely on the binding pocket residues. It should also be noted that several studies<sup>32,34,35</sup> have provided evidence of functional redundancy in the YTHDF family. According to this model, a pan-human-YTHDF inhibitor may be more advantageous than a selective one since the inhibition of only one of the three YTHDF proteins would be compensated by the presence of the other two.<sup>35</sup>

Here we report 17 fragment binders of the YTHDF2 reader [Figures 2, 3; Table 1]. A homogeneous time-resolved fluorescence (HTRF)-based assay<sup>36</sup> and X-ray crystallography were used to quantify the affinity and determine the binding mode (the descriptions of the HTRF assay and the crystal optimization process are reported in the Supporting Information). The 17 binders were identified from a pool of about 30 fragments. Ligands **1**–**8** were identified among previously reported<sup>29</sup> and putative YTHDC1 binders, while ligands **9**–**17** originated from structure-based design. Compounds **2**–**4**, **7**, and **8** were synthesized in-house, while the remaining fragments were procured from Chemspace.

The 17 ligands are four derivatives of m<sup>6</sup>adenine (we do not abbreviate m<sup>6</sup>adenine to distinguish the nucleobase from the nucleoside m<sup>6</sup>A), four pyrazolopyrimidine derivatives, seven

Table 1. 2D Structures and Affinity of m<sup>6</sup>A and the 17 Fragment-Like Ligands of the m<sup>6</sup>A Reader Domain of YTHDF2 [The NH group that is involved as hydrogen bond donor to the backbone carbonyl of C433 is emphasized (blue). Data for the m<sup>6</sup>A reader domain of YTHDC1 are shown as a basis of comparison (red).]

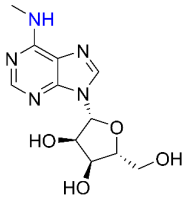
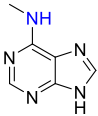
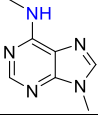
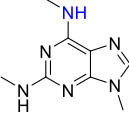
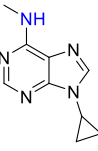
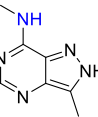
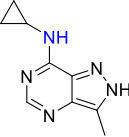
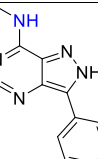
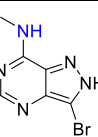
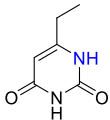
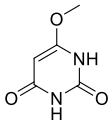
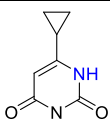
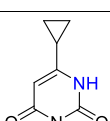
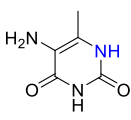
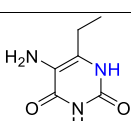
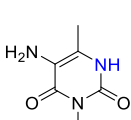
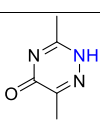
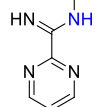
Compound nr.	2D structure	Residual signal at 1 mM concentration <sup>a</sup>	IC <sub>50</sub> [μM] <sup>b</sup> (LE <sup>c</sup> )	PDB code (Resolution [Å])
m <sup>6</sup> A		100% 32%	504	4RDN <sup>7</sup> (2.10) 6ZCN <sup>30</sup> (1.6)
m <sup>6</sup> adenine derivatives				
1		75% 49%		7YWB (2.01)
2		74% 23%	306	7Z7B (1.80) 7P8A <sup>29</sup> (1.7)
3		ND*		7Z7F (1.95)
4		96% 19%	294	7Z54 (1.82) 7P8B <sup>29</sup> (1.2)
Pyrazolopyrimidine derivatives				
5		42% 3%	410 (0.38) 39 (0.50)	7Z5M (1.70) 7P8F <sup>29</sup> (1.5)
6		75% 49%		7Z8W (1.90)
7		18% 28%	161 (0.30) 142	7YXE (1.85)
8		59% 31%		7Z8P (1.97)

Table 1. continued

Compound nr.	2D structure	Residual signal at 1 mM concentration <sup>a</sup>	IC <sub>50</sub> [μM] <sup>b</sup> (LE <sup>c</sup> )	PDB code (Resolution [Å])
Uracil derivatives				
9		62% 79%		7YX6 (1.80)
10		73% 91%		7Z8X (1.96)
11		12% 72%	174 (0.47)	7R5W (1.75)
12		32% 61%	491 (0.38)	7Z4U (1.83)
13		81% 90%		7R5F (2.00)
14		77% 87%		7Z93 (1.97)
15		83% 98%		7Z92 (1.91)
Others				
16		78% 89%		7R5L (1.70)
17		76% 87%		7ZG4 (2.01)

<sup>a</sup>The residual signal at 1 mM compound concentration is measured using an HTRF-based binding assay as previously reported.<sup>36</sup> The signal decreases (with respect to buffer-only measurement) when the fragment competes with the binding of the natural ligand, i.e., m<sup>6</sup>A-oligoRNA. Thus, the lower the signal, the higher the affinity of the fragment. The reported values are the average of ≥2 biological replicates; each replicate is the average of two technical replicates. <sup>b</sup>The IC<sub>50</sub> value for the YTHDF2 reader domain was measured only for the fragments that are able to decrease the signal by more than 50% at a concentration of 1 mM. <sup>c</sup>Ligand efficiency calculated according to  $LE = -\frac{\Delta G}{n_{HA}} \approx -RT \frac{\ln IC_{50}}{n_{HA}}$ . \* indicates not measured because of poor solubility.

uracil derivatives, and two derivatives of triazine and pyrimidine, respectively [Table 1 and Figure 3]. The overlap of the 17 structures gives a flavor of the flexibility of the binding site residues as well as of the diversity of the fragments and the extent of the tridimensional exploration of the YTHDF2 binding site [Figure 2A,B]. It should be noted that, differently from what was previously observed for

YTHDC1,<sup>26</sup> the 17 binders shown in this study are rather planar. This is a direct consequence of the narrowness of the YTHDF binding site. Accordingly, the YTHDF2 binding site and binding loop show limited plasticity, and only Y418 and W491 display side-chain flexibility. A smaller and more rigid binding pocket is one of the features that makes the YTHDF2 reader, as well as YTHDF1 and YTHDF3, more difficult

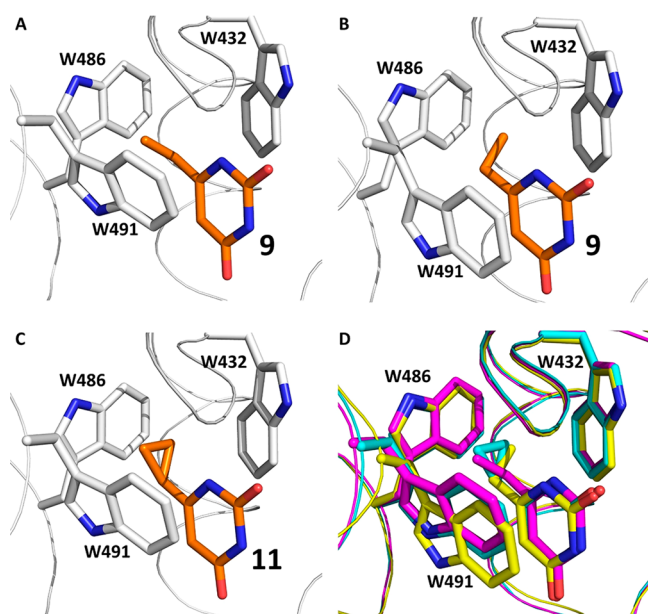


**Figure 4.** Orientations of the ethyl and cyclopropyl groups of compounds **9** and **11** (carbon atoms in orange in panels A–C) in the tryptophan cage of the YTHDF2 reader domain (carbon atoms in gray). Compound **9** in complex with (A) chain A and (B) chain B of YTHDF2. (C) Compound **11** in complex with YTHDF2. (D) Structural overlap of the two binding modes of compound **9** (carbon atoms in magenta and yellow, respectively) and compound **11** (cyan).

targets than the YTHDC1 reader, for which 58 ligands have already been disclosed.<sup>26,29,30</sup>

At the beginning of our search for YTHDF2 ligands, we decided to neglect selectivity against other YTH readers. Thus, we started from the hypothesis that  $m^6$ adenine derivatives and heteroaromatics with similar spatial arrangements of polar groups would bind to the tryptophan cage of the YTHDF  $m^6$ A-RNA readers. We first evaluated small sets of derivatives of  $m^6$ adenine and of the  $m^6$ adenine-isosteric pyrazolopyrimidine scaffold which we had previously identified as a binder of the YTHDC1 reader domain.<sup>29</sup> As expected,  $m^6$ adenine (compound **1**) shows the same position, orientation, and hydrogen-bonding pattern [Figure 3A] as the nucleobase of  $m^6$ A-RNA [Figure S2]. There is a hydrogen bond between the N7 in the adenine ring and a structural water molecule that is involved as a hydrogen bond acceptor and donor with the side chains of W432 and D528, respectively. The conserved water and water-bridged polar interactions are present in all the available YTHDF2 structures. The position and the interactions of the conserved water molecule are identical in YTHDF1 and YTHDF3 (PDB codes: 4RCJ and 6ZOT).

Compounds **2** and **3** are N9-methyl derivatives of  $m^6$ adenine (compound **1**) while compound **4** has a cyclopropyl at N9. In all these fragments the alkyl group is in a favorable position to interact with the side chain of Y418 through a  $\pi$ -alkyl interaction. Nonetheless, the Y418 side chain seems to assume a favorable orientation only for ligand **3** and in the chain B of the structure of YTHDF2 in complex with ligand **4**. Compound **3** is also characterized by a secondary amine in position C2. The amino group acts as a hydrogen bond donor toward the side chain of D422. Unfortunately, the effect of this additional interaction on the potency of **3** could not be evaluated because of the poor solubility of the compound. Overall, the four derivatives of  $m^6$ adenine (group 1) are

characterized by low potency. At 1 mM fragment concentration, the residual signal ranges from 74% to almost 100% with respect to DMSO buffer solution [Table 1]. This reflects the very scarce potency shown by  $m^6$ A, which is not able to reduce the emitted signal even at high concentrations [Table 1]. These observations point toward the necessity of moving on from an  $m^6$ A-derived warhead to explore other scaffolds.

The pyrazolopyrimidine derivatives **5**–**8** maintain all the interactions already observed for  $m^6$ adenine. In addition,  $N^2$ -H acts as a hydrogen bond donor toward the side chain of D528 [Figure 3B]. The C3-methyl derivative **5** is the simplest compound of this series and shows  $IC_{50} = 410 \mu M$  for the YTHDF2 reader [Figure 5A] and weak affinity for YTHDF1 and YTHDF3 [Table S1]. The substitution of the methyl with a cyclopropyl has a detrimental effect on the potency of ligand **6** which is lower than the one observed for its parent compound **5** [Table 1]. The crystal structure of YTHDF2 in complex with ligand **6** (PDB code: 7Z8W) shows two radically different poses. The poorer affinity of ligand **6** is consistent with the two binding modes which indicate lower enthalpic stabilization. In chain B, ligand **6** shows a binding mode comparable to the one observed for **5** with the cyclopropyl inside the aromatic cage [Figure S3A]. In chain A, ligand **6** is oriented with the cyclopropyl ring pointing outside toward the side chain of Y418 while the methyl group is in the cage [Figure S3B]. This binding pose, along with what was previously observed for compounds **2**–**4** encouraged the exploration of groups able to interact more strongly with the Y418 side chain. It should be noted that the residue Y418 is present in YTHDF1, YTHDF2, and YTHDF3, whereas the corresponding residue is an asparagine (N363) in YTHDC1.<sup>33</sup> The phenyl substituent at C3 in compound **7** [Scheme S1] interacts through  $\pi$ - $\pi$  stacking with the side chain of Y418 [Figure 3C]. Its  $IC_{50}$  value of  $161 \mu M$  for YTHDF2 [Figure 5A] is 2.5 times more favorable than the one of **5** [Table 1], and it shows modest selectivity against YTHDF1 and YTHDF3 [Table S1]. We also measured the affinity of compound **8** [Scheme S1] which features a bromine on its C3. The presence of the Br atom in **8** does not show additional interactions nor any improvement in potency with respect to the methyl of **5** [Table 1].

In parallel to the characterization of the  $m^6$ adenine and pyrazolopyrimidine derivatives, we noticed that the N1 and ethyl substituent of compound **9** can mimic the interactions of  $N^6$  and the methyl group of  $m^6$ adenine, respectively [Figure 3A, D]. Thus, we designed manually 15 compounds and used molecular dynamics simulations (see Methods in the Supporting Information) to assess the structural stability of the manually docked binding poses [Figure S4]. Nine of the 15 compounds were stable during the simulations and were evaluated *in vitro*. The methoxy of 6-methoxyuracil (**10**) does not provide higher affinity [Table 1]. In contrast, a closer look at the two different orientations of the ethyl tail of compound **9** in chains A and B of the crystal structure [Figure 4A,B], suggested to improve the interactions with the bottom of the aromatic cage by replacing the ethyl group with a cyclopropyl. Gratifyingly, the crystal structure of compound **11** (6-cyclopropyluracil) confirmed our design [Figures 3E and 4C]. Compound **11** shows  $IC_{50} = 174 \mu M$  [Figure 5A] and has a very favorable ligand efficiency of  $0.47 \text{ kcal mol}^{-1}$  per non-hydrogen atom, which makes it a good fragment-like hit.<sup>37</sup> The hit **11** binds also to the reader domains of YTHDF1 and

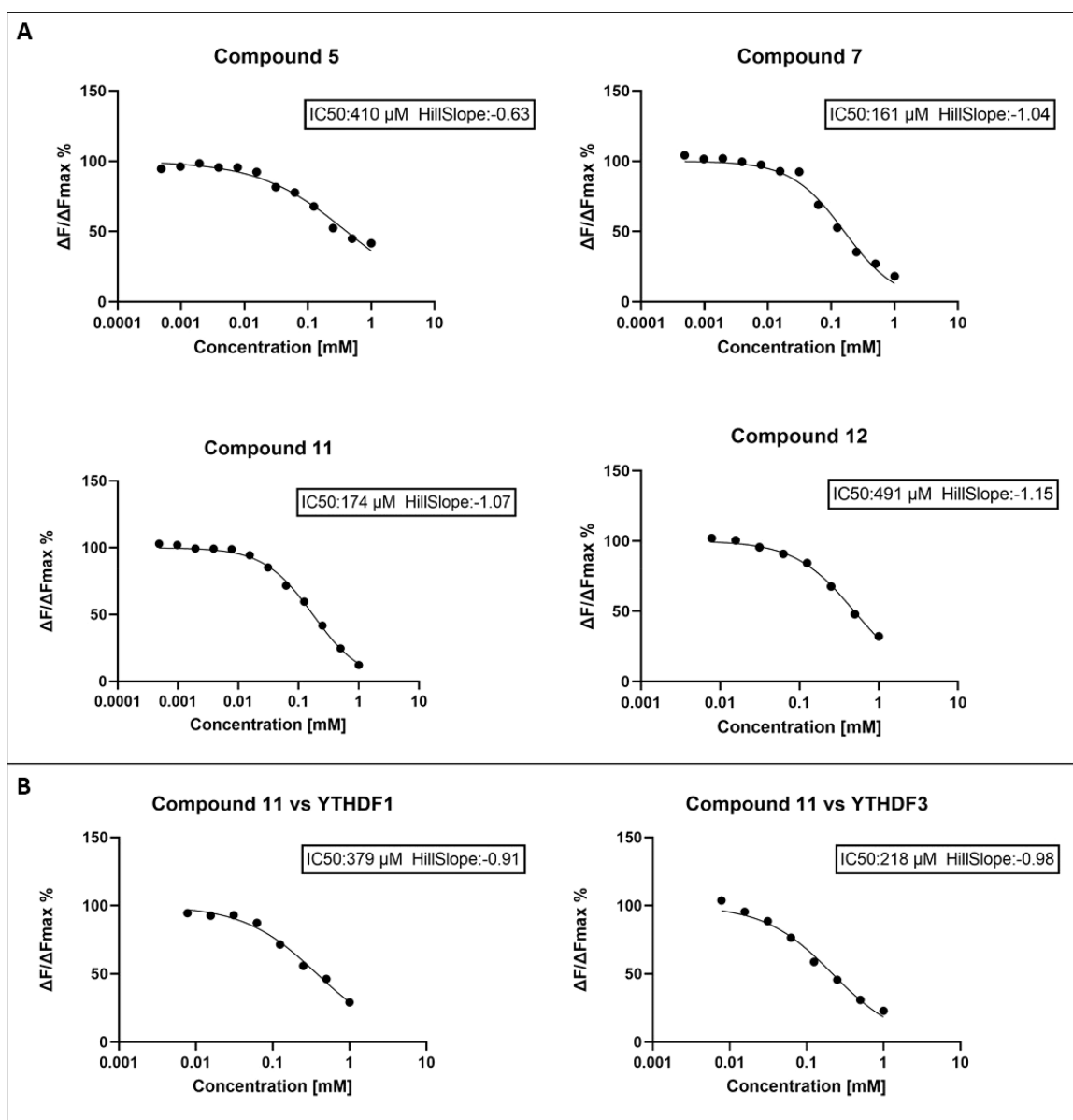


**Figure 5.** (A) HTRF dose–response curves for YTHDF2. Only the compounds with a residual signal at 1 mM lower than 50% were measured. (B) Dose–response curves of compound 11 for YTHDF1 (left) and YTHDF3 (right). The data points are the average of  $\geq 2$  biological replicates, each replicate is the average of two technical replicates.

YTHDF3 ( $IC_{50} = 379$  and  $218 \mu M$ , respectively [Figure 5B]), whereas it is selective against YTHDC1 ( $IC_{50} > 1$  mM).

Although compound 11 displays a poorer H-bonding pattern than 13 (three vs four hydrogen bonds) the affinity of 11 for YTHDF2 is substantially higher [Table 1]. Thus, the potency of 11 is likely due to the favorable interactions of the cyclopropyl group with the tryptophan residues of the cage. The comparison with compound 9 (ethyl in the cage) provides further evidence of the favorable contribution of the cyclopropyl of 11 [Figure 4D]. Concerning potential substituents at N3 of the uracil ring, methylation at N3 results in a poorer  $IC_{50}$  value ( $491 \mu M$  for compound 12 vs  $174 \mu M$  for 11). The methyl group of 12 points toward the carbonyl oxygen of K416, which results in a less favorable interaction with respect to the NH of compound 11.

The crystal structure of the YTHDF2 complex with 11 [Figure 3E] shows that the C5 of 6-cyclopropyluracil is at a distance of  $3.2 \text{ \AA}$  from one of the two oxygen atoms in the side

chain of D422. Thus, we expected a higher affinity of the 5-aminouracil derivatives 13–15. The additional  $-\text{NH}_2$  group at position C5 of the uracil ring does not improve the affinity despite the favorable polar interactions with the side chain of D422 [Figure 3F]. One possible explanation is that, upon binding, the unfavorable desolvation of the  $-\text{NH}_2$  group of the ligand and carboxyl group of D422 is not fully compensated by the polar interactions.

The triazine derivative 16 interacts through hydrogen bonds with the backbone carbonyl of C433, the amide NH of Y418, and the conserved water [Figure 3G]. An interesting feature of this structure is the position of the side chain of W491 which interacts with the triazine ring assuming an orientation that is almost perpendicular to the one normally observed. This conformation is indeed more similar to the “close” conformation that can be observed for YTHDF2 in the unbound state (PDB code: 4RDO).<sup>7</sup> A comparable conformation of the W491 side chain can only be observed in

chain A of the structure with compound 15. Considering the conformational flip observed upon m<sup>6</sup>A binding,<sup>7</sup> the flexibility of this side chain is not surprising. Nonetheless, it is the first time that this conformation is reported for YTHDF proteins in the bound state.

In compound 17 the pyrimidine scaffold is functionalized with a methylamidine group on C2. The latter group is positively charged (pK<sub>a</sub> = 8.5, as calculated with MarvinSketch 21.20.0, ChemAxon, (<http://www.chemaxon.com>)) and is involved in electrostatic interactions with the side chain of D422 and the backbone carbonyl of C433 as well as cation- $\pi$  interactions with W486 and W432 [Figure 3H]. Moreover, the pyrimidine ring is involved in a stacking interaction with W491. A residual signal higher than 70% implies that neither compound 16 nor 17 shows significant binding, even at a concentration of 1 mM. Nonetheless, the investigation of these two scaffolds increases the extent of the presented chemical space exploration.

In conclusion, we have identified and characterized by protein crystallography the first (to the best of our knowledge) small-molecule ligands of the m<sup>6</sup>A-reader domain of YTHDF2. Furthermore, we present the first structure of YTHDF2 in complex with an RNA oligonucleotide which provides further evidence of the similar m<sup>6</sup>A recognition mechanism of the three human YTHDF readers [Figure 1]. Some of the ligands interact with the side chains of D528 [Figure 3B, C] and D422 [Figure 3F] which are not directly involved in the binding of the natural ligand. We also identified the side chain of Y418, at the entrance of the aromatic cage, as a potential target for improving the potency [Figure 3C]. The most ligand-efficient compound, 6-cyclopropyluracil (11), has IC<sub>50</sub> = 174  $\mu$ M [Figure 5A] and a ligand efficiency of 0.47 kcal mol<sup>-1</sup> per non-hydrogen atom. Thus, it is an interesting fragment-like hit for further optimization of the potency for the YTHDF2 reader or for the three human YTHDF readers as they share an almost identical m<sup>6</sup>A recognition site.

The 17 crystal structures presented in this work are at high resolution [Figure S5] and thus provide useful information for hit optimization. Compound 11 could be functionalized at C5 with an -NH<sub>2</sub> group, permitting a hydrogen bond formation with D422 as observed for compound 13 [Figure 3F]. The phenyl of compound 7 could be replaced by heteroaromatic rings. Furthermore, as the phenyl ring points toward the entrance of the m<sup>6</sup>A recognition pocket [Figure 3C], decorations of the ring could be explored to catch polar interactions with the solvent-exposed residues.

## ■ ASSOCIATED CONTENT

### SI Supporting Information

The Supporting Information is available free of charge at <https://pubs.acs.org/doi/10.1021/acsmmedchemlett.2c00303>.

Materials and methods, HTRF dose-response curves, structural overlap of YTHDF2 in complex with m<sup>6</sup>Adenine and m<sup>6</sup>A-oligoRNA, orientations of 6 in the YTHDF2 binding pocket, stability of the predicted pose during molecular dynamics simulations, electron density maps of eight fragments, YTHDF1/3 selectivity measurements, NMR spectra, and HPLC traces of final compounds, including Figures S1–S5 and Table S1 (PDF)

X-ray data collection and refinement statistics for the 18 complex YTH-YTHDF2 crystal structures (XLSX)

## ■ AUTHOR INFORMATION

### Corresponding Authors

Yaozong Li – Department of Biochemistry, University of Zurich, CH-8057 Zurich, Switzerland; Department of Chemistry, Umeå University, SE-901 87 Umeå, Sweden; [orcid.org/0000-0002-5796-2644](https://orcid.org/0000-0002-5796-2644); Email: [y.li@bioc.uzh.ch](mailto:y.li@bioc.uzh.ch)

Amedeo Cafilisch – Department of Biochemistry, University of Zurich, CH-8057 Zurich, Switzerland; [orcid.org/0000-0002-2317-6792](https://orcid.org/0000-0002-2317-6792); Phone: +41 44 635 5521; Email: [cafilisch@bioc.uzh.ch](mailto:cafilisch@bioc.uzh.ch)

### Authors

Francesco Nai – Department of Biochemistry, University of Zurich, CH-8057 Zurich, Switzerland; [orcid.org/0000-0002-4258-3174](https://orcid.org/0000-0002-4258-3174)

Raed Nachawati – Department of Biochemistry, University of Zurich, CH-8057 Zurich, Switzerland; [orcid.org/0000-0001-9516-2552](https://orcid.org/0000-0001-9516-2552)

František Zálešák – Department of Biochemistry, University of Zurich, CH-8057 Zurich, Switzerland

Xiang Wang – Department of Biochemistry, University of Zurich, CH-8057 Zurich, Switzerland

Complete contact information is available at: <https://pubs.acs.org/10.1021/acsmmedchemlett.2c00303>

### Notes

The authors declare no competing financial interest.

## ■ ACKNOWLEDGMENTS

We thank Pablo Andres Vargas-Rosales, Annalisa Invernizzi, and Francesco Errani for helpful suggestions and interesting discussions. We thank Beat Blattmann at the Protein Crystallization Center (University of Zürich) for assistance with crystallization screening. We thank the Swiss National Supercomputing Center in Lugano and the Swedish National Infrastructure for Computing for providing the computational resources. We thank the scientists at the Swiss Light Source at Paul Scherrer Institute for the support before and during the X-ray crystallography data acquisition. This work was supported by the International Postdoc Grant funded by the Swedish Research Council (Grant VR 2019-00608 to Y.L.) and an Excellence grant of the Swiss National Science Foundation (310030B\_189363 to A.C.).

## ■ ABBREVIATIONS

YTHDF2, YT521-B homology domain family 2; m<sup>6</sup>A, N<sup>6</sup>-methyladenosine; YTHDC1, YTH domain containing 1; METTL3–14, methyltransferase-like 3–14; oligoRNA, oligoribonucleotide; HTRF, homogeneous time-resolved fluorescence; LE, ligand efficiency

## ■ REFERENCES

- (1) Saletore, Y.; Meyer, K.; Korlach, J.; Vilfan, I. D.; Jaffrey, S.; Mason, C. E. The Birth of the Epitranscriptome: Deciphering the Function of RNA Modifications. *Genome Biol.* **2012**, *13* (10), 175.
- (2) Shi, H.; Wei, J.; He, C. Where, When, and How: Context-Dependent Functions of RNA Methylation Writers, Readers, and Erasers. *Mol. Cell* **2019**, *74* (4), 640–650.
- (3) Dominissini, D.; Moshitch-Moshkovitz, S.; Schwartz, S.; Salmon-Divon, M.; Ungar, L.; Osenberg, S.; Cesarkas, K.; Jacob-Hirsch, J.; Amariglio, N.; Kupiec, M.; Sorek, R.; Rechavi, G. Topology of the



Human and Mouse M6A RNA Methylomes Revealed by M6A-Seq. *Nature* **2012**, *485* (7397), 201–206.

(4) Zhu, T.; Roundtree, I. A.; Wang, P.; Wang, X.; Wang, L.; Sun, C.; Tian, Y.; Li, J.; He, C.; Xu, Y. Crystal Structure of the YTH Domain of YTHDF2 Reveals Mechanism for Recognition of N6-Methyladenosine. *Cell Res.* **2014**, *24* (12), 1493–1496.

(5) Wang, X.; Lu, Z.; Gomez, A.; Hon, G. C.; Yue, Y.; Han, D.; Fu, Y.; Parisien, M.; Dai, Q.; Jia, G.; Ren, B.; Pan, T.; He, C. N6-Methyladenosine-Dependent Regulation of Messenger RNA Stability. *Nature* **2014**, *505* (7481), 117–120.

(6) Liu, S.; Li, G.; Li, Q.; Zhang, Q.; Zhuo, L.; Chen, X.; Zhai, B.; Sui, X.; Chen, K.; Xie, T. The Roles and Mechanisms of YTH Domain-Containing Proteins in Cancer Development and Progression. *Am. J. Cancer Res.* **2020**, *10* (4), 1068–1084.

(7) Li, F.; Zhao, D.; Wu, J.; Shi, Y. Structure of the YTH Domain of Human YTHDF2 in Complex with an m(6)A Mononucleotide Reveals an Aromatic Cage for m(6)A Recognition. *Cell Res.* **2014**, *24* (12), 1490–1492.

(8) Du, H.; Zhao, Y.; He, J.; Zhang, Y.; Xi, H.; Liu, M.; Ma, J.; Wu, L. YTHDF2 Destabilizes M6A-Containing RNA through Direct Recruitment of the CCR4–NOT Deadenylation Complex. *Nat. Commun.* **2016**, *7* (1), 12626.

(9) Zhang, C.; Chen, Y.; Sun, B.; Wang, L.; Yang, Y.; Ma, D.; Lv, J.; Heng, J.; Ding, Y.; Xue, Y.; Lu, X.; Xiao, W.; Yang, Y.-G.; Liu, F. M6A Modulates Haematopoietic Stem and Progenitor Cell Specification. *Nature* **2017**, *549* (7671), 273–276.

(10) Yu, R.; Li, Q.; Feng, Z.; Cai, L.; Xu, Q. M6A Reader YTHDF2 Regulates LPS-Induced Inflammatory Response. *Int. J. Mol. Sci.* **2019**, *20* (6), 1323.

(11) Chen, C.-Y. A.; Shyu, A.-B. Mechanisms of Deadenylation-Dependent Decay. *Wiley Interdiscip. Rev. RNA* **2011**, *2* (2), 167–183.

(12) Chen, M.; Wei, L.; Law, C.-T.; Tsang, F. H.-C.; Shen, J.; Cheng, C. L.-H.; Tsang, L.-H.; Ho, D. W.-H.; Chiu, D. K.-C.; Lee, J. M.-F.; Wong, C. C.-L.; Ng, I. O.-L.; Wong, C.-M. RNA N6-Methyladenosine Methyltransferase-like 3 Promotes Liver Cancer Progression through YTHDF2-Dependent Posttranscriptional Silencing of SOCS2. *Hepatology* **2018**, *67* (6), 2254–2270.

(13) Zhang, C.; Huang, S.; Zhuang, H.; Ruan, S.; Zhou, Z.; Huang, K.; Ji, F.; Ma, Z.; Hou, B.; He, X. YTHDF2 Promotes the Liver Cancer Stem Cell Phenotype and Cancer Metastasis by Regulating OCT4 Expression via M6A RNA Methylation. *Oncogene* **2020**, *39* (23), 4507–4518.

(14) Li, J.; Meng, S.; Xu, M.; Wang, S.; He, L.; Xu, X.; Wang, X.; Xie, L. Downregulation of N6-Methyladenosine Binding YTHDF2 Protein Mediated by MiR-493–3p Suppresses Prostate Cancer by Elevating N6-Methyladenosine Levels. *Oncotarget* **2018**, *9* (3), 3752–3764.

(15) Li, J.; Xie, H.; Ying, Y.; Chen, H.; Yan, H.; He, L.; Xu, M.; Xu, X.; Liang, Z.; Liu, B.; Wang, X.; Zheng, X.; Xie, L. YTHDF2 Mediates the mRNA Degradation of the Tumor Suppressors to Induce AKT Phosphorylation in N6-Methyladenosine-Dependent Way in Prostate Cancer. *Mol. Cancer* **2020**, *19* (1), 152.

(16) Hua, Z.; Wei, R.; Guo, M.; Lin, Z.; Yu, X.; Li, X.; Gu, C.; Yang, Y. YTHDF2 Promotes Multiple Myeloma Cell Proliferation via STAT5A/MAP2K2/p-ERK Axis. *Oncogene* **2022**, *41* (10), 1482–1491.

(17) Einstein, J. M.; Perelis, M.; Chaim, I. A.; Meena, J. K.; Nussbacher, J. K.; Tankka, A. T.; Yee, B. A.; Li, H.; Madrigal, A. A.; Neill, N. J.; Shankar, A.; Tyagi, S.; Westbrook, T. F.; Yeo, G. W. Inhibition of YTHDF2 Triggers Proteotoxic Cell Death in MYC-Driven Breast Cancer. *Mol. Cell* **2021**, *81* (15), 3048–3064.e9.

(18) Wang, J.; Lu, A. The Biological Function of M6A Reader YTHDF2 and Its Role in Human Disease. *Cancer Cell Int.* **2021**, *21* (1), 109.

(19) Paris, J.; Morgan, M.; Campos, J.; Spencer, G. J.; Shmakova, A.; Ivanova, I.; Mapperley, C.; Lawson, H.; Wotherspoon, D. A.; Sepulveda, C.; Vukovic, M.; Allen, L.; Sarapuu, A.; Tavoranis, A.; Guitart, A. V.; Villacreces, A.; Much, C.; Choe, J.; Azar, A.; van de Lagemaat, L. N.; Vernimmen, D.; Nehme, A.; Mazurier, F.; Somerville, T. C. P.; Gregory, R. I.; O'Carroll, D.; Kranc, K. R.

Targeting the RNA M6A Reader YTHDF2 Selectively Compromises Cancer Stem Cells in Acute Myeloid Leukemia. *Cell Stem Cell* **2019**, *25* (1), 137–148.e6.

(20) Liu, J.; Yue, Y.; Han, D.; Wang, X.; Fu, Y.; Zhang, L.; Jia, G.; Yu, M.; Lu, Z.; Deng, X.; Dai, Q.; Chen, W.; He, C. A METTL3–METTL14 Complex Mediates Mammalian Nuclear RNA N6-Adenosine Methylation. *Nat. Chem. Biol.* **2014**, *10* (2), 93–95.

(21) Xie, H.; Li, J.; Ying, Y.; Yan, H.; Jin, K.; Ma, X.; He, L.; Xu, X.; Liu, B.; Wang, X.; Zheng, X.; Xie, L. METTL3/YTHDF2 M6A Axis Promotes Tumorigenesis by Degrading SETD7 and KLF4 MRNAs in Bladder Cancer. *J. Cell. Mol. Med.* **2020**, *24* (7), 4092–4104.

(22) Zhou, D.; Tang, W.; Xu, Y.; Xu, Y.; Xu, B.; Fu, S.; Wang, Y.; Chen, F.; Chen, Y.; Han, Y.; Wang, G. METTL3/YTHDF2 M6A Axis Accelerates Colorectal Carcinogenesis through Epigenetically Suppressing YPEL5. *Mol. Oncol.* **2021**, *15* (8), 2172–2184.

(23) Xu, Q.-C.; Tien, Y.-C.; Shi, Y.-H.; Chen, S.; Zhu, Y.-Q.; Huang, X.-T.; Huang, C.-S.; Zhao, W.; Yin, X.-Y. METTL3 Promotes Intrahepatic Cholangiocarcinoma Progression by Regulating IFIT2 Expression in an M6A-YTHDF2-Dependent Manner. *Oncogene* **2022**, *41* (11), 1622–1633.

(24) Moroz-Omori, E. V.; Huang, D.; Kumar Bedi, R.; Cheriyanunnell, S. J.; Bochenkova, E.; Dolbois, A.; Rzczkowski, M. D.; Li, Y.; Wiedmer, L.; Cafilisch, A. METTL3 Inhibitors for Epitranscriptomic Modulation of Cellular Processes. *ChemMedChem* **2021**, *16* (19), 3035–3043.

(25) Yankova, E.; Blackaby, W.; Albertella, M.; Rak, J.; De Braekeleer, E.; Tsagkogeorga, G.; Pilka, E. S.; Aspris, D.; Leggate, D.; Hendrick, A. G.; Webster, N. A.; Andrews, B.; Fosbeary, R.; Guest, P.; Irigoyen, N.; Eleftheriou, I.; Gozdecka, M.; Dias, J. M. L.; Bannister, A. J.; Vick, B.; Jeremias, I.; Vassiliou, G. S.; Rausch, O.; Tzelepis, K.; Kouzarides, T. Small-Molecule Inhibition of METTL3 as a Strategy against Myeloid Leukaemia. *Nature* **2021**, *593* (7860), 597–601.

(26) Bedi, R. K.; Huang, D.; Wiedmer, L.; Li, Y.; Dolbois, A.; Wojdyla, J. A.; Sharpe, M. E.; Cafilisch, A.; Sledz, P. Selectively Disrupting M6A-Dependent Protein–RNA Interactions with Fragments. *ACS Chem. Biol.* **2020**, *15* (3), 618–625.

(27) Bedi, R. K.; Huang, D.; Eberle, S. A.; Wiedmer, L.; Ślędz, P.; Cafilisch, A. Small-Molecule Inhibitors of METTL3, the Major Human Epitranscriptomic Writer. *ChemMedChem* **2020**, *15* (9), 744–748.

(28) Dolbois, A.; Bedi, R. K.; Bochenkova, E.; Müller, A.; Moroz-Omori, E. V.; Huang, D.; Cafilisch, A. 1,4,9-Triazaspiro[5.5]Undecan-2-One Derivatives as Potent and Selective METTL3 Inhibitors. *J. Med. Chem.* **2021**, *64* (17), 12738–12760.

(29) Li, Y.; Bedi, R. K.; Nai, F.; von Roten, V.; Dolbois, A.; Zálešák, F.; Nachawati, R.; Huang, D.; Cafilisch, A. Structure-Based Design of Ligands of the M6A-RNA Reader YTHDC1. *Eur. J. Med. Chem. Rep.* **2022**, *5*, 100057.

(30) Li, Y.; Bedi, R. K.; Wiedmer, L.; Sun, X.; Huang, D.; Cafilisch, A. Atomistic and Thermodynamic Analysis of N6-Methyladenosine (M6A) Recognition by the Reader Domain of YTHDC1. *J. Chem. Theory Comput.* **2021**, *17* (2), 1240–1249.

(31) Liao, S.; Sun, H.; Xu, C. YTH Domain: A Family of N6-Methyladenosine (m6A) Readers. *Genomics Proteomics Bioinformatics* **2018**, *16* (2), 99–107.

(32) Li, Y.; Bedi, R. K.; Moroz-Omori, E. V.; Cafilisch, A. Structural and Dynamic Insights into Redundant Function of YTHDF Proteins. *J. Chem. Inf. Model.* **2020**, *60* (12), 5932–5935.

(33) Xu, C.; Liu, K.; Ahmed, H.; Loppnau, P.; Schapira, M.; Min, J. Structural Basis for the Discriminative Recognition of N6-Methyladenosine RNA by the Human YTS21-B Homology Domain Family of Proteins. *J. Biol. Chem.* **2015**, *290* (41), 24902–24913.

(34) Lasman, L.; Krupalnik, V.; Viukov, S.; Mor, N.; Aguilera-Castrejon, A.; Schneir, D.; Bayerl, J.; Mizrahi, O.; Peles, S.; Tawil, S.; Sathe, S.; Nachshon, A.; Shani, T.; Zerbib, M.; Kilimnik, I.; Aigner, S.; Shankar, A.; Mueller, J. R.; Schwartz, S.; Stern-Ginossar, N.; Yeo, G. W.; Geula, S.; Novershtern, N.; Hanna, J. H. Context-Dependent

Functional Compensation between Ythdf M6A Reader Proteins. *Genes Dev.* **2020**, *34*, 1373.

(35) Zaccara, S.; Jaffrey, S. R. A Unified Model for the Function of YTHDF Proteins in Regulating M6A-Modified mRNA. *Cell* **2020**, *181* (7), 1582–1595.e18.

(36) Wiedmer, L.; Eberle, S. A.; Bedi, R. K.; Śledź, P.; Caflich, A. A Reader-Based Assay for M6A Writers and Erasers. *Anal. Chem.* **2019**, *91* (4), 3078–3084.

(37) Schultes, S.; de Graaf, C.; Haaksma, E. E. J.; de Esch, I. J. P.; Leurs, R.; Krämer, O. Ligand Efficiency as a Guide in Fragment Hit Selection and Optimization. *Drug Discovery Today Technol.* **2010**, *7* (3), e157–e162.

## Recommended by ACS

### Small-Molecule Ebselen Binds to YTHDF Proteins Interfering with the Recognition of N<sup>6</sup>-Methyladenosine-Modified RNAs

Mariachiara Micaelli, Alessandro Provenzani, *et al.*

SEPTEMBER 14, 2022

ACS PHARMACOLOGY & TRANSLATIONAL SCIENCE

READ 

### Discovery of a Novel Small-Molecule Inhibitor Disrupting TRBP–Dicer Interaction against Hepatocellular Carcinoma via the Modulation of microRNA Biogenesis

Ting Peng, Fei Wang, *et al.*

JUNE 13, 2022

JOURNAL OF MEDICINAL CHEMISTRY

READ 

### Design and Characterization of a Natural Arf-GEFs Inhibitor Prodrug CHNQD-01255 with Potent Anti-Hepatocellular Carcinoma Efficacy *In Vivo*

Yao-Yao Jiang, Chang-Lun Shao, *et al.*

SEPTEMBER 11, 2022

JOURNAL OF MEDICINAL CHEMISTRY

READ 

### Structure–Activity Relationship and Neuroprotective Activity of 1,5-Dihydro-2H-naphtho[1,2-*b*][1,4]diazepine-2,4(3H)-diones as P2X<sub>4</sub> Receptor Antagonists

Kiran S. Toti, Kenneth A. Jacobson, *et al.*

SEPTEMBER 23, 2022

JOURNAL OF MEDICINAL CHEMISTRY

READ 

Get More Suggestions >